*Journal of Low Temperature Physics, Vol. 68, Nos. 1/2, 1987*

# Superconducting Tunneling without the Tunneling Hamiltonian. II. Subgap Harmonic Structure

**Gerald B. Arnold**

*Department of Physics, University of Notre Dame, Notre Dame, Indiana*

(Received December 12, 1986)

*The theory of superconducting tunneling without the tunneling Hamiltonian is extended to treat superconductor/insulator/superconductor junctions in which the transmission coefficient of the insulating barrier approaches unity. The solution for the current in such junctions is obtained by solving the problem of a particle hopping in a one-dimensional lattice of sites, with forward and reverse transfer integrals that depend on the site. The results are applied to the problem of subgap harmonic structure in superconducting tunneling. The time-dependent current at finite voltage through a junction exhibiting subgap structure is found to have terms that oscillate at all integer multiples of the Josephson frequency,* $n(2eV/\hbar)$*. The amplitudes of these new, and as yet unmeasured, ac current contributions as a function of voltage are predicted.*

## 1. INTRODUCTION

The behavior of superconducting tunneling junctions that have nearly transparent barriers has been of continuing interest to experimentalists. Such junctions exhibit nonideal current versus voltage curves (e.g., leakage current), which are not explained by the standard transfer (or tunneling) Hamiltonian model. Indeed, to some extent, "good" junctions are experimentally defined to be those that exhibit $I-V$ characteristics consistent with the predictions of the transfer Hamiltonian theory. Such junctions typically are a small fraction of the junctions actually made.

In order to understand the behavior of this larger class of nonideal junctions, one requires a theory that goes beyond the lowest order in the transmission probability $T^2$. The transfer Hamiltonian approach is *designed* to treat only the lowest order in $T^2$. In refs. 1 and 2, I presented a theory that solves the problem of the tunneling current in superconducting junctions exactly, i.e., to all orders in $T^2$. It is based on the approach developed by Feuchtwang.[3] The method is actually a realization of Bardeen's original



0022-2291/87/0700-0001$05.00/0 

idea[4] for calculating the tunneling current, by using nonequilibrium Green's functions and the equations of motion. Because the results are expressed in terms of Green's functions, they are convenient for calculating the influence of many-body self-energy effects on the tunneling current, especially in situations where the tunnel barrier is nearly transparent.

In ref. 2, I presented results for the Josephson zero-bias current, and for the $I-V$ characteristics of junctions with one electrode in the normal state. The appearance of leakage current and behavior of the Josephson critical current as a function of barrier transmission probability were explored in detail.

In this work, I will present theoretical results for the tunneling $I-V$ characteristics of superconductor/insulator/superconductor (SIS) junctions with ultrathin barriers. These characteristics display structure *below* the voltage that corresponds to the sum of energy gaps, in contrast to the prediction of the transfer Hamiltonian theory.[5] The structure in the dynamical resistance $dV/dI$ has been called "subgap harmonic structure" because there are peaks at voltages that (roughly) correlate with gap energies divided by integers. This structure was first observed by Taylor and Burstein[6] and independently by Adkins.[7] Despite the fact that it has been observed and studied for more than 20 years, this structure has not been quantitatively described by any theory. The calculations of $dV/dI$ presented in this work reproduce the experimental results for this structure with an accuracy not attained by any previous theories. The accuracy of this calculation may enable one to separate contributions to $dV/dI$ arising from low barrier effects and those arising from Josephson self-coupling,[8] a competing explanation for subgap harmonic structure, which relies on the nonlinear coupling of Josephson radiation with the oscillating Josephson current that produces this radiation to produce a dc component of current below the sum of gaps.

For several years, one popular explanation of subgap structure was that of multiparticle tunneling (MPT), first presented by Schrieffer and Wilkins.[9] Recently, an alternative explanation was proposed by Klapwijk, Blonder, and Tinkham (KBT).[10] This alternative explanation involves a mechanism called Andreev reflection.[11] I will argue in this work that the KBT picture of subgap structure is essentially equivalent to the MPT picture. However, I believe that the KBT picture is preferable because it is capable of describing not only the appearance of threshold voltages for peaks in $dV/dI$, but also the background leakage current of the junction, in more detail than the MPT picture. Further reasons for preferring the KBT description are:

1. The KBT mechanism applies to excess currents in junctions in which one electrode is normal, but MPT does not. In other words, the KBT mechanism is more generally applicable.

2. The precise nature of the mechanism by which Cooper pairs are broken up in MPT is not directly dealt with. For the KBT explanation, this mechanism (Andreev reflection) is the *foundation* of the whole explanation.

The equivalence of the two pictures lies in the observation that Andreev reflection involves pair generation and pair breaking in the two electrodes (in fact, it explains it), and this pair generation and breaking is the basis for the MPT picture.

A single example will illustrate the above remarks. Consider an SIS junction at a voltage slightly below $2\Delta/2$, where $2\Delta$ is the energy gap in each S electrode (cf. Fig. 1). Measure energy relative to the chemical potential in the right electrode. At the energy $-\delta$ there exists a nonvanishing probability for finding a particle at the barrier/right electrode interface, because there is particle amplitude there. For brevity I will call this an "evanescent hole" at energy $-\delta$, because this energy corresponds to a hole energy in the normal state of the right electrode. Of course, in the barrier, there is really no distinction between electrons and holes, because it is an insulator. Andreev reflection of the hole occurs at the interface (there can be no particle transmission into the superconducting right electrode at this energy), destroying a Cooper pair in the right electrode by filling the hole with one member of the pair, leaving the other electron of the pair at energy $\delta$, traveling to the left as an evanescent electron. In the view of the left electrode, however, this evanescent wave is a *hole*, because it is at an energy $(\Delta - 2\delta)$ below the left electrode chemical potential. Thus, a similar Andreev reflection of this hole occurs at the left electrode/barrier interface, destroying a Cooper pair in the left electrode, leaving an evanescent electron of energy $\Delta - 2\delta$ above the chemical potential of the left electrode, i.e., at energy $2\Delta - 3\delta$. The evanescent electron travels to the right, tunneling into allowed unoccupied states in the right electrode. Note that there are two extra traversals of the barrier region, making the amplitude for the occurrence of this process of order $(T^2)^2$ in the single-particle tunneling probability $T^2$. Note that there can be no interference between reflected evanescent waves in the barrier, because, being evanescent, these waves are pure nonoscillating exponentials. Thus, even at a voltage $\Delta - \delta$, there will be current through this SIS junction, of an amount governed by the magntidue of $(T^2)^2$.

In the MPT picture, the factor $(T^2)^2$ arises because two particles tunnel through the barrier. However, this process cannot occur until the voltage reaches $\Delta$, because there are no allowed states for the two particles of the Cooper pair in the left electrode at energy $\Delta - \delta$. Hence, MPT cannot explain the behavior of the leakage current below $\Delta$.

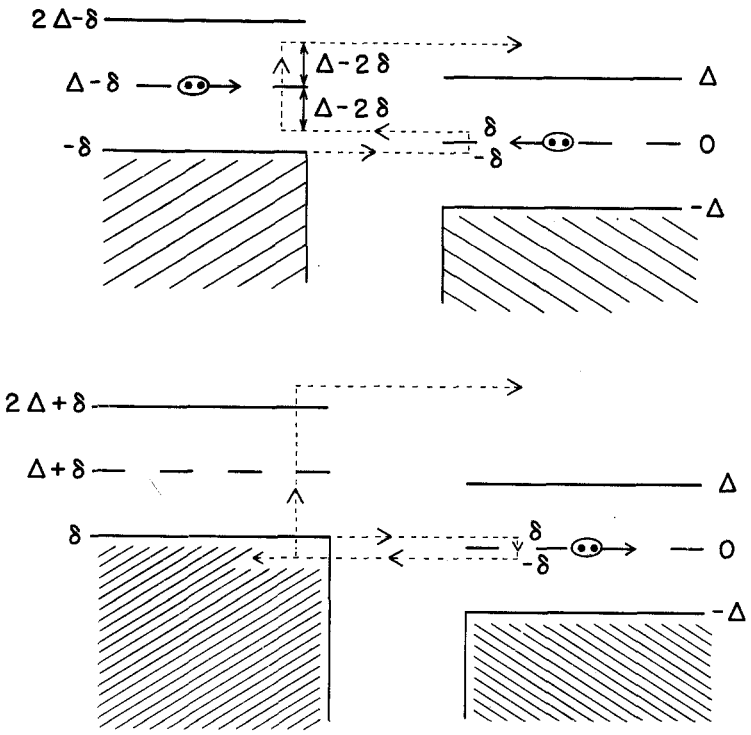


Fig. 1. Top: The semiconductor picture for SIS tunneling at a voltage $\Delta - \delta$ and zero temperature. The dashed lines indicate the path of a particle that tunnels from the top of the occupied (shaded) states in the left electrode and Andreev-reflects twice, emerging into allowed unoccupied levels in the right electrode. Bottom: For a voltage $\Delta + \delta$, at which there is one complete Andreev reflection and a final, but partial, Andreev reflection.

For a voltage slightly above $\Delta$ (at $\Delta + \delta$) MPT says that Cooper pairs can tunnel directly into the right electrode with probability $(T^2)^2$, yielding supercurrent. In the KBT picture this supercurrent is produced by recognizing that now the evanescent particle incident from the left is at an energy above the chemical potential of the right electrode, making it an evanescent electron. It can *form* a Cooper pair by taking an evanescent particle from the left electrode at energy $-\delta$. This yields a Cooper pair in the right electrode, propagating to the right as supercurrent, and an evanescent hole, tunneling to the left, finding allowed (for holes) states on the left, and also partially Andreev-reflecting symmetrically across the chemical potential of the left electrode, thereby partially destroying some Cooper pair amplitude in the left electrode.

Partial Andreev reflection for $|E| > \Delta$ can occur because the coefficient for Andreev reflection[10] is

$$\left| \frac{1}{E/\Delta + [(E/\Delta)^2 - 1]^{1/2}} \right|^2 \tag{1}$$

Thus, even for $E/\Delta = 1.3$, approximately 50% of the incoming particle amplitude is still Andreev-reflected.

If we summarize the result of the processes discussed above, we note that at voltage $\Delta - \delta$, an electron incoming from the left tunnels through the barrier via Andreev reflection-assisted tunneling, and produces a net electronic current $-e$ traveling from left to right. At voltage $\Delta + \delta$, the incoming electron now generates a pair (supercurrent) traveling from left to right, in addition to partial hole current from right to left, and partial electron current from left to right, yielding $-e + (-2e)$ total charge current traveling from left to right. Thus, at the threshold voltage $\Delta$, pair current appears, as in MPT. While the KBT explanation is more complex, it provides a more comprehensive description of the pair-breaking and generation processes involved in the tunneling.

In Section 2, I present the model and its assumptions, and in Section 3, I review results from refs. 1 and 2 and introduce the notation I will use. Section 4 presents the result for the current through an SIS′ junction, and in Section 5, I outline the approach I have taken toward solving for the current numerically. In Sections 6 and 7, I discuss my results for the dc current versus voltage for symmetric and asymmetric junctions, and in Section 8, I present results for the ac current versus voltage contributions, and predict the appearance of these terms, which, to my knowledge, have never been measured by any experiment. Finally, in Section 9, I present some discussion and conclusions.

## 2. THE MODEL

The model junction consists of two semi-infinite superconducting electrodes with a planar, structureless barrier sandwiched between. By "structureless' I mean that the density of states in the barrier vanishes throughout the range of energies $|E| \ll U_B$, where $U_B$ is the equilibrium value of the barrier height above the chemical potential in the junction, and $E$ is energy as measured relative to the equilibrium chemical potential. In this work, only energies of the order of a milli-electron volt are of interest, so $U_B$ need only be greater than about 50 meV. In such a case, the trapezoidal shape of the barrier under an applied voltage is negligible, so the barrier shape may be taken to be rectangular, to a good approximation, at all voltages of interest. Effects arising from the capacitance of the junction are neglected.

When a voltage $V$ is applied, the entire voltage drop is assumed to occur across the barrier. It is also assumed that the quasiparticles in each electrode are distributed according to the Fermi distribution, with chemical potentials that differ by $Ve$ ($e$ is the electron charge). It is not necessary to assume that the electrodes are described by equilibrium Fermi distributions, but it does simplify the treatment, and avoids the introduction of extraneous features into the description of the physics I will study. I will restrict my calculations to zero temperature, although this restriction can be relaxed quite easily.

## 3. NOTATION AND GREEN'S FUNCTIONS

I will not repeat derivations already presented in ref. 2, but, in order to write in compact form the equations to be studied and solved, I will summarize some results of that work and introduce some notation in this section.

The Pauli matrices are denoted by $\tau_1$, $\tau_2$, and $\tau_3$. Often-used combinations of these are

$$P_\pm = \tfrac{1}{2}(1 \pm \tau_3), \qquad \tau_\pm = \tfrac{1}{2}(\tau_1 \pm i\tau_2) \tag{2}$$

I will set $\hbar = 1$, $2m = 1$, and measure wavevectors in terms of

$$k_{Fx} = (k_F^2 - k_\parallel^2)^{1/2} \tag{3}$$

where $k_\parallel$ is the magnitude of quasiparticle wavevector component parallel to the interfaces and $k_F$ is the magnitude of the Fermi wavevector, assumed to be the same for both electrodes.

To a function $\Gamma(t, t')$ I will associate an operator $\Gamma$ such that

$$\langle t|\Gamma|t'\rangle = \Gamma(t, t') \qquad \text{where} \quad \langle t|t'\rangle = \delta(t - t') \tag{4}$$

The Fourier coefficients corresponding to this function in energy space are $\Gamma(E, E')$ and may be symbolically represented as a matrix element

$$\langle E|\Gamma|E'\rangle = \Gamma(E, E') \qquad \text{where} \quad \langle E|E'\rangle = \delta(E - E') \tag{5}$$

and

$$\langle t|E\rangle = e^{iEt}/(2\pi)^{1/2} \tag{6}$$

Thus, for example,

$$\langle E|\Gamma G|E'\rangle = \int dE''\Gamma(E, E'')G(E'', E') \tag{7}$$

In the rest of this section, I will list those results from ref. 2 that are necessary for this work.

For the left (L) and right (R) electrode Green's functions, one has

$$\langle E|g^r_{L,R}|E'\rangle = \delta(E-E')g^r_{L,R}(E) \tag{8}$$

and

$$g^r_{L,R}(E) = i[\varepsilon^r_{L,R}(E) + \delta^r_{L,R}(E)\tau_1] \tag{9}$$

$$\varepsilon^r_{L,R}(E) = \begin{cases} \dfrac{|E|}{[E^2-\Delta_{L,R}(E)^2]^{1/2}}, & |E|>\Delta_{L,R}(E) \\ \dfrac{E}{[\Delta_{L,R}(E)^2-E^2]^{1/2}}, & \Delta_{L,R}(E)>|E| \end{cases} \tag{10}$$

$$\delta^r_{L,R}(E) = [\Delta_{L,R}(E)/E]\varepsilon^r_{L,R}(E) \tag{11}$$

where $\Delta_{L,R}(E)$ is the superconducting pair potential in the left or right electrode. The superscript "r" refers to retarded functions. Advanced functions are indicated by the superscript "a," and are equal to the adjoints of the above expressions. By convention, functions without a superscript are to be interpreted as *either* advanced or retarded.

From Eq. (81) of ref. 2

$$\tilde{g}_R = e^{i(\phi/2)\tau_3} g_R e^{-i(\phi/2)\tau_3} \tag{12}$$

where the exponentials are "phase difference operators" introduced above Eq. (45) of ref. 2, and

$$\begin{aligned} \langle E|\tilde{g}_R|E'\rangle &= \delta(E-E')[g_R(E-eV)_{11}P_+ + g_R(E+eV)_{22}P_-] \\ &\quad + \delta(E-E'-\omega_0)e^{i\phi_0}g_R(E-eV)_{12}\tau_+ \\ &\quad + \delta(E-E'+\omega_o)e^{-i\phi_0}g_R(E+eV)_{21}\tau_- \\ &= \sum_{s=-1,0,1} \delta(E-E'+s\omega_0)\tilde{g}_R(E, E+s\omega_0) \end{aligned} \tag{13}$$

Here $\omega_0 = 2eV$ is the Josephson frequency, and $\phi_0$ is the equilibrium value of the Josephson phase difference between left and right electrodes.

Because the quasiparticles in each electrode are assumed to be distributed according to the Fermi function $f(E)$,

$$\langle E|g^<_{L,R}|E'\rangle = \delta(E-E')g^<_{L,R}(E) \tag{14}$$

$$g^<_{L,R}(E) = [g^a_{L,R}(E) - g^r_{L,R}(E)]f(E) \tag{15}$$

and

$$\tilde{g}^<_R = e^{i(\phi/2)\tau_3} g^<_R e^{-i(\phi/2)\tau_3} \tag{16}$$

The matrix element

$$\langle E|\tilde{g}^<_R|E'\rangle \tag{17}$$

is obtained from Eq. (13) by replacing $g_R$ by $g^<_R$.

For the structureless barrier

$$g_{BL} = g_{BR} = -(1/\kappa)\coth(\kappa d_B)\tau_3 \tag{18}$$

$$T^2 = [\kappa^2 \sinh^2(\kappa d_B) + \cosh^2(\kappa d_B)]^{-1} \tag{19}$$

where $d_B$ is the barrier thickness and (in ordinary units)

$$\kappa = (2mU_B/\hbar^2 - k_\parallel^2)^{1/2}/k_{Fx} \tag{20}$$

My calculations indicate that the dependence of $\kappa$ on $k_\parallel$ does not lead to significant effects upon the tunneling current. This means that the tunneling current can be calculated at the most important value of $k_\parallel$, $k_\parallel = 0$, because the integration over all $k_\parallel$ values leads to no significantly different results.

Some useful adjoint relations are

$$[\tilde{g}_R^<]^\dagger = -\tilde{g}_R^<, \qquad [g_L^<]^\dagger = -g_L^< \tag{21}$$

$$[\tilde{g}_R^r]^\dagger = \tilde{g}_R^a, \qquad [g_L^r]^\dagger = g_L^a \tag{22}$$

## 4. THE CURRENT

The derivation in ref. 2 supplies the following expression for the current at time $t$ [Eq. (83)]:

$$I(L, t) = 2e \sum_{k_\parallel} T^2 \langle t | \mathrm{Tr}\{P[\tilde{g}_R^r \tilde{\Gamma}_L^< - \tilde{\Gamma}_L^< \tilde{g}_R^a + \tilde{g}_R^< \tilde{\Gamma}_L^a - \tilde{\Gamma}_L^r \tilde{g}_R^<]\} | t \rangle \tag{23}$$

The trace "Tr" is a trace in the two-dimensional space of the Pauli matrices and

$$\tilde{\Gamma}_L^< = -\tilde{\Gamma}_L^r [g_L^< + T^2 \tilde{g}_R^<] \tilde{\Gamma}_L^a \tag{24}$$

where

$$M(E)\tilde{\Gamma}_L(E, E') + J^-(E)\tilde{\Gamma}_L(E - \omega_0, E') + J^+(E)\tilde{\Gamma}_L(E + \omega_0, E') = \delta(E - E') \tag{25}$$

with

$$M(E) = g_L(E) + g_{BL} - T^2 g_{BR} + T^2 g_R(E - eV)_{11} P_+ + T^2 g_R(E + eV) P_- \tag{26}$$

$$J^-(E) = T^2 e^{i\phi_0} g_R(E - eV)_{12} \tau_+ \tag{27}$$

$$J^+(E) = T^2 e^{-i\phi_0} g_R(E + eV)_{21} \tau_- \tag{28}$$

Using

$$\tilde{\Gamma}_L^a = (\tilde{\Gamma}_L^r)^\dagger, \qquad (\tilde{\Gamma}_L^<)^\dagger = -\tilde{\Gamma}_L^< \tag{29}$$

and the adjoint relations at the end of the previous section, we can express the current more compactly as

$$I(L, t) = \mathrm{Re}[J(T)] = \mathrm{Re}\left\{4e \sum_{k_\parallel} T^2 \langle t | \mathrm{Tr}[P_+(\tilde{g}_R^r \tilde{\Gamma}_L^< + \tilde{g}_R^< \tilde{\Gamma}_L^a)] | t \rangle\right\} \quad (30)$$

where I introduce the *complex* time-dependent current $J(t)$.

The energy representation is most useful for the calculations to be performed, so I will calculate

$$J(t) = 4e \sum_{k_\parallel} T^2 \int \frac{dE}{2\pi} \int dE' e^{i(E'-E)t} \langle E' | \mathrm{Tr}[P_+(\tilde{g}_R^r \tilde{\Gamma}_L^< + \tilde{g}_R^< \tilde{\Gamma}_L^a)] | E \rangle \quad (31)$$

Use of Eq. (13) of the previous section yields

$$\begin{aligned} J(t) = 4e \sum_{k_\parallel} T^2 \int \frac{dE}{2\pi} \int dE' e^{i(E'-E)t} \\ \times \sum_{s=-1,0,1} \mathrm{Tr}\{P_+[\tilde{g}_R^r(E, E+s\omega_0)\tilde{\Gamma}_L^<(E+s\omega_0, E') \\ + \tilde{g}_R^<(E, E+s\omega_0)\tilde{\Gamma}_L^a(E+s\omega_0, E')]\} \end{aligned} \quad (32)$$

The evaluation of this expression requires the solution of Eq. (25) for $\tilde{\Gamma}_L$.

It is evident from the equation for $\tilde{\Gamma}_L(E, E')$ that the energy difference $E - E'$ in the solution will be an integer multiple of $\omega_0$, i.e., the solution for $\tilde{\Gamma}_L(E, E')$ will be a sum of terms, each proportional to a delta function:

$$\tilde{\Gamma}_L(E, E') = \sum_n \delta(E - E' + n\omega_0)\tilde{\Gamma}_L(E, E + n\omega_0) \quad (33)$$

where $n$ is any positive or negative integer, or zero. It is useful at this point to introduce a matrix notation:

$$\tilde{\Gamma}_L(E, E + n\omega_0) = \tilde{\Gamma}_L(E)_{0n}, \qquad \tilde{\Gamma}_L(E + m\omega_0, E + n\omega_0) = \tilde{\Gamma}_L(E)_{mn} \quad (34)$$

$$\tilde{g}_R^r(E, E + s\omega_0) = \tilde{g}_R^r(E)_{0s}, \qquad \delta_{mn} g_L^<(E + m\omega_0) = g_L^<(E)_{mn} \quad (35)$$

In this notation, Eq. (32) becomes

$$\begin{aligned} J(t) = -4e \sum_{k_\parallel} T^2 \int \frac{dE}{2\pi} \sum_{n,s} \mathrm{Tr}\Bigg[ P_+\Bigg\{ \sum_{ms'} \tilde{g}_R^r(E)_{0s} \tilde{\Gamma}_L^r(E)_{sm} [g_L^<(E)_{mm+s'} \\ + T^2 g_R^<(E)_{mm+s'}] \tilde{\Gamma}_L^a(E)_{m+s'n} - \tilde{g}_R^<(E)_{0s} \tilde{\Gamma}_L^a(E)_{sn} \Bigg\} \Bigg] e^{in\omega_0 t} \end{aligned} \quad (36)$$

(The sums over $s$ and $s'$ include only $-1$, 0, and 1, while the sums over $n$ and $m$ include all integers.)

Thus, the exact solution for $J(t)$ is in the form of a Fourier series:

$$J(t) = \sum_n e^{in\omega_0 t} J_n(\omega_0) \tag{37}$$

At zero bias ($\omega_0 = 0$)

$$J(t) = \sum_n J_n(0) \tag{38}$$

yields the Josephson current discussed at length in ref. 2. This can be obtained exactly because $\omega_0 = 0$ in Eq. (25), so

$$\tilde{\Gamma}_L(E, E') = [M(E) + J^-(E) + J^+(E)]^{-1} \delta(E - E') \tag{39}$$

At finite bias, there is evidently no exact solution for $\tilde{\Gamma}_L$. In the next section, I will outline a method for obtaining an approximate solution.

## 5. SOLVING THE EQUATION FOR $\tilde{\Gamma}_L$

Using the notation introduced at the end of the last section, I find that Eq. (25) becomes

$$M(E)_{00}\tilde{\Gamma}_L(E)_{0n} + J^-(E)_{0-1}\tilde{\Gamma}_L(E)_{-1n} + J^+(E)_{01}\tilde{\Gamma}_L(E)_{1n} = \delta_{0n} \tag{40}$$

If I replace $E$ by $E + m\omega_0$ in Eq. (25), then the corresponding equation in the new notation is

$$M(E)_{mm}\tilde{\Gamma}_L(E)_{mn} + J^-(E)_{mm-1}\tilde{\Gamma}_L(E)_{m-1n} + J^+(E)_{mm+1}\tilde{\Gamma}_L(E)_{m+1n} = \delta_{mn} \tag{41}$$

where

$$M(E)_{mm} = g_L(E + m\omega_0) + g_{BL} - T^2 g_{BR} + T^2 g_R(E + m\omega_0 + eV)_{11} P_+ + T^2 g_R(E + m\omega_0 + eV)_{22} P_- \tag{42}$$

$$J^+(E)_{mm+1} = T^2 e^{-i\phi_0} g_R(E + m\omega_0 + eV)_{21} \tau_- \tag{43}$$

$$J^-(E)_{mm-1} = T^2 e^{i\phi_0} g_R(E + m\omega_0 - eV)_{12} \tau_+ \tag{44}$$

Upon inspection, one notes that $\tilde{\Gamma}_L(E)_{mn}$ is analogous to a $2 \times 2$ matrix propagator for a particle hopping from the $m$th site in a one-dimensional lattice to the $n^{\text{th}}$ site in the lattice, with a matrix transfer integral of $J^+(E)$ in the forward direction and $J^-(E)$ in the backward direction.

I have solved this problem numerically by *truncating* the one-dimensional lattice to $2N+1$ sites, where $N$ is adjusted until the results are insensitive to any further increase in $N$. The smaller $\kappa d_B$ is, the larger

is $T^2$ (but $T^2$ is always less than unity), so $N$ must be larger for smaller $\kappa d_B$ values. Thus, $\tilde{\Gamma}_L$ becomes a $(2N+1)\times(2N+1)$ matrix of $2\times 2$ matrices, or a $(4N+2)\times(4N+2)$ matrix. The truncated equation (41) may now be solved exactly by finding the inverse of the (tridiagonal) matrix that acts upon $\tilde{\Gamma}_L$.

The subscripts on $\tilde{\Gamma}_L$, $\tilde{g}_R$, etc., do not indicate the actual matrix elements, because, for example, $\tilde{\Gamma}_L(E)_{mn}$ is a $2\times 2$ matrix itself. I will use *superscripts* to designate the actual matrix elements, so that, for example,

$$\tilde{\Gamma}_L(E)^{ij}$$

is the element in the $i$th row, $j$th column of the matrix $\tilde{\Gamma}_L(E)$.

To summarize, for each energy $E$, I will truncate all matrices so that each has dimension $4N+2$, and numerically solve for $\tilde{\Gamma}_L(E)^{jk}$ in

$$\sum_{j=1}^{4N+2} L(E)^{ij}\tilde{\Gamma}_L(E)^{jk} = \delta^{ik} \tag{45}$$

where

$$L(E) = M(E) + J^-(E) + J^+(E) \tag{46}$$

The results will be used in the expression for the $n$th Fourier coefficient of the complex current:

$$J_n(\omega_0) = 4e\sum_{k_\parallel} T^2 \int \frac{dE}{2\pi} \sum_{j=2N}^{2N+2} [\tilde{g}_R^r(E)^{2N+1,j}\tilde{\Gamma}_L^<(E)^{j,2N+2n+1} + \tilde{g}_R^<(E)^{2N+1,j}\tilde{\Gamma}_L^a(E)^{j,2N+2n+1}] \tag{47}$$

where

$$\tilde{\Gamma}_L^<(E)^{jk} = -\sum_{m=1}^{4N+2}\sum_{p=m-1}^{m+1} \tilde{\Gamma}_L^r(E)^{jm}[g_L^<(E)^{mp} + T^2\tilde{g}_R^<(E)^{mp}]\tilde{\Gamma}_L^a(E)^{pk} \tag{48}$$

In these expressions, I have used the fact that $g_L^<$, $\tilde{g}_R^<$, and $\tilde{g}_R^r$ are tridiagonal matrices, and have chosen the central site [$n=0$ in Eq. (41)] to correspond to the new matrix indices $2N+1$ and $2N+2$.

## 6. NUMERICAL RESULTS FOR SYMMETRIC JUNCTIONS

For a symmetric junction, all energies may be scaled to the energy gap, so that the only variable parameter is $T^2$, the transmission probability, a dimensionless quantity that characterizes the transparency of the barrier. The value of $N$ chosen for these calculations was $N=4$. The range of the

$E$ integral in Eq. (47) was chosen to be $-4 \leq E \leq 4$, where $E$ is measured in units of the energy gap, and the gaps were given an imaginary part equal to 2% of the gap. Values chosen for $T^2$ ranged from 0.13 to 0.95. The value of the phase difference at zero voltage $\phi_0$ was chosen to be that which maximized the zero-bias Josephson current, although the finite-voltage current appeared to have very weak dependence on $\phi_0$, so that $\phi_0 = \pi/2$ would have given essentially the same results for $\mathrm{Re}[J_0(\omega_0)]$.

Figure 2 shows the $\mathrm{Re}[J_0(\omega_0)]$ versus voltage curves for various values of $T^2$. Steplike structures in these curves become more pronounced as $T^2$ decreases (i.e., as barrier transparency decreases), although the subgap current, naturally, decreases in magnitude as $T^2$ decreases.

Figure 3 gives the corresponding $dV/dI$ curves. The subgap peaks in $dV/dI$ sharpen and increase in magnitude as $T^2$ decreases, while, at the same time, the number of subgap peaks decreases. It is interesting to note that the positions of these peaks *do not* correlate precisely with values of $2\Delta/n$ ($n$ = integer).

In Fig. 4, values of $2\Delta/n$ up to $n = 9$ are indicated by vertical lines in the $dV/dI$ versus $V$ curves for $T^2 = 0.42$. The peaks are seen to shift their positions relative to the $2\Delta/n$ lines. Their occurrence is related to phenomena that depend upon $2\Delta/n$, but these phenomena combine to produce structures shifted relative to $2\Delta/n$ because the current depends in a *nonlinear* way

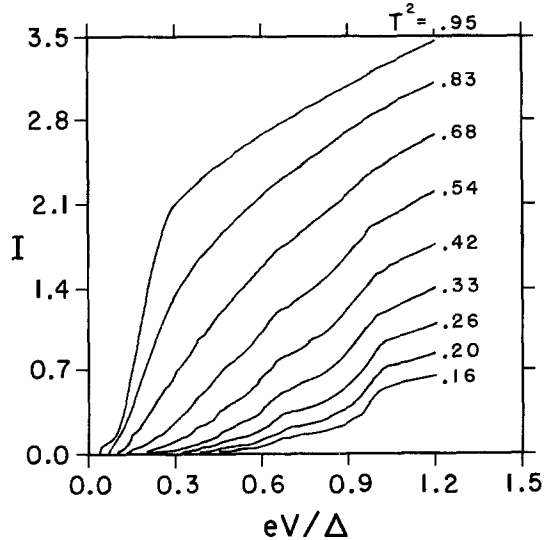


Fig. 2. The tunneling current versus voltage for an SIS junction with an insulating barrier characterized by a transmission parameter, $T^2$ between 0.16 and 0.95.

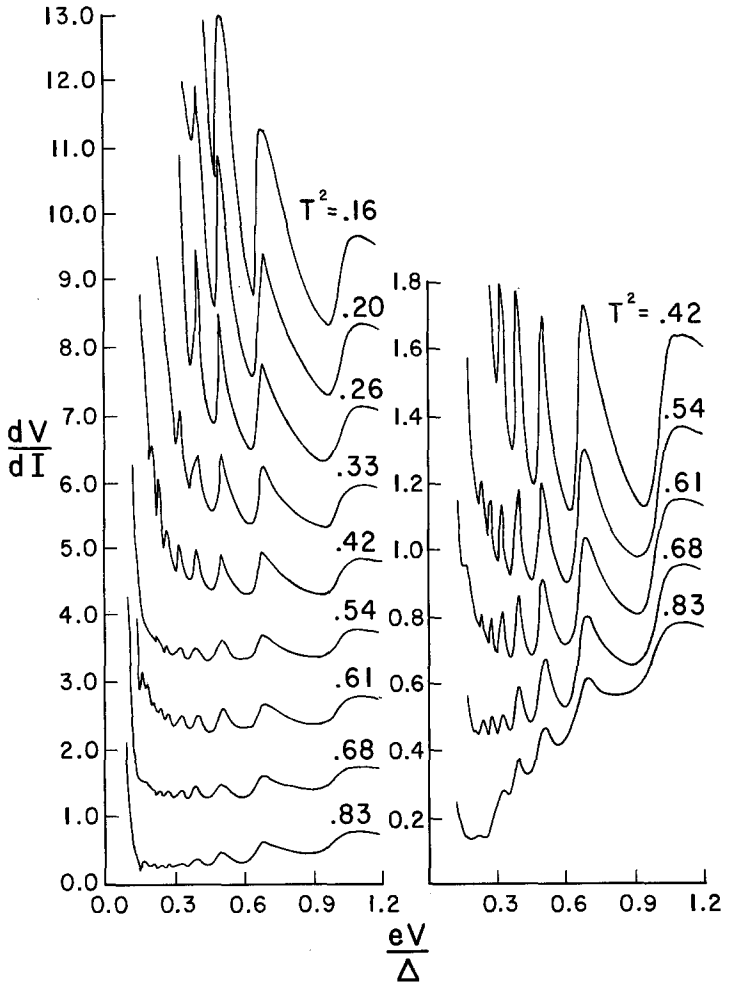


Fig. 3. Dynamical resistance $dV/dI$ versus voltage for the $I$ versus $V$ curves of Fig. 2. Units along the vertical are arbitrary.

upon the solutions for $\tilde{\Gamma}_L$. This shifting of subgap peaks in $dV/dI$ relative to $2\Delta/n$ has been observed experimentally by Bermon[12] and by Gaffney and Tomasch.[13]

As noted in the introduction, in the KBT description the peaks arise from multiple Andreev reflections of evanescent particles in the thin barrier. A particle incident upon a region where the superconducting pair potential increases will have part of its amplitude (or all of its amplitude, if it is

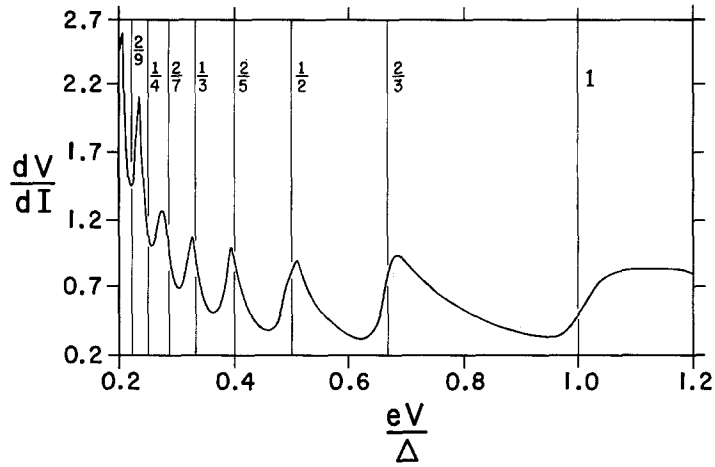


Fig. 4. Dynamical resistance versus voltage for an SIS junction with $T^2 = 0.42$. The values of $eV/\Delta$ corresponding to $eV = 2\Delta/n$, $n$ = integer, are indicated by vertical lines. Units along the vertical are arbitrary.

incident at an energy lying between the pair potential and the Fermi level) reflected as hole amplitude at an energy that is symmetrically located beneath the Fermi level. An incoming hole amplitude can also be reflected as particle amplitude, in a mirror image of this process. This Andreev reflection of particle amplitude into hole amplitude (or vice versa) arises due to pairing (or depairing) at the interface, where the gap has a steplike increase: incident particle amplitude above the chemical potential pairs with particle amplitude at an energy symmetrically beneath the chemical potential, producing Cooper pair amplitude, which then propagates at the chemical potential as supercurrent. A hole is thereby left behind, so that the result of Andreev reflection is the conversion of incident particle amplitude to supercurrent and reflected hole amplitude. Similarly, incident hole amplitude destroys some Cooper pair amplitude, and reflects as particle amplitude.

The symmetrical SIS junction provides two identical gaps on either side of the barrier, hence two pair potential increases that can Andreev-reflect the evanescent incoming amplitudes of particles or holes within the barrier. Figure 5 indicates the situation when the bias voltage is infinitesimally greater than $2\Delta/2$, at zero temperature. A particle may tunnel through the barrier from the left, Andreev-reflect across the Fermi level on the right as a hole, and return again to Andreev-reflect on the left, across the left electrode Fermi level, then tunneling through to be detected as particle current. In the process, some Cooper pair amplitude is generated in the right superconductor, yielding a supercurrent from left to right, and

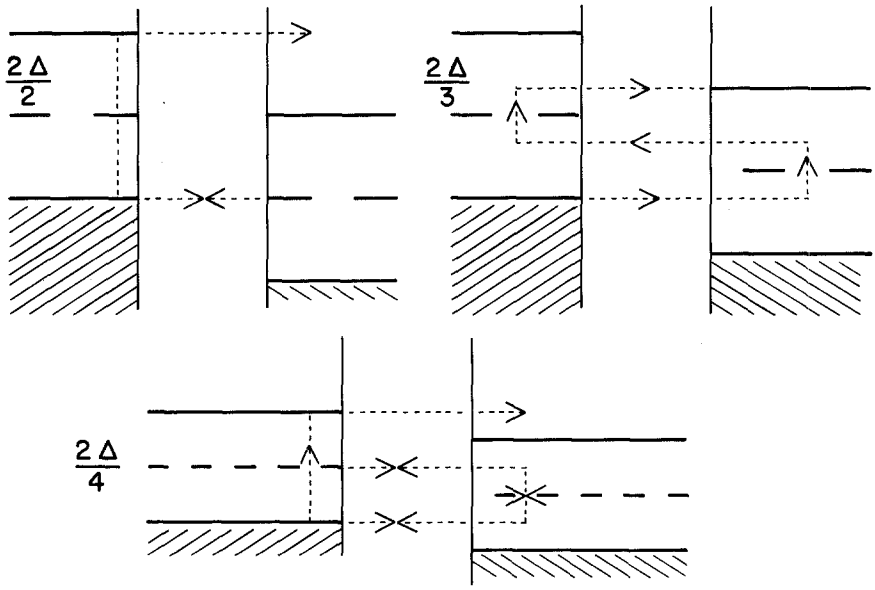


Fig. 5. Semiconductor picture of tunneling at $eV = \Delta$, $2\Delta/3$, and $2\Delta/4$, showing paths of tunneling particle in energy, with Andreev reflections (vertical dashed lines) indicated.

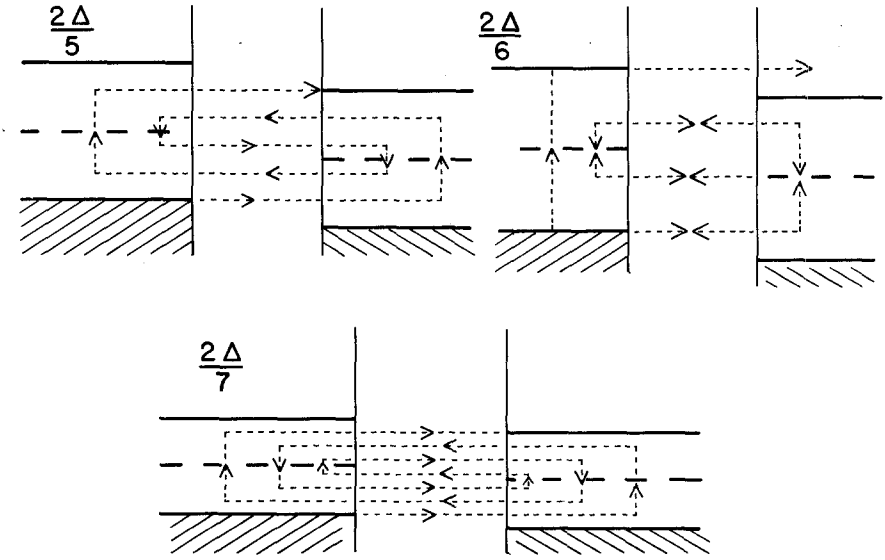


Fig. 6. Semiconductor picture of tunneling at $eV = 2\Delta/5$, $2\Delta/6$, $2\Delta/7$, showing the character of the multiple Andreev reflections involved in the higher order processes at these voltages.

some (less) supercurrent is destroyed in the left electrode. Three traversals of the barrier region are required for this process; hence, this process is of order $(T^2)^2$, where $T^2$ is the single-particle tunneling probability. Obviously, such a process will occur for all voltages between $2\Delta/2$ and $2\Delta$. However, note that at $2\Delta/2$ the tunneling particle enters the high density of states at $-\Delta$ in the left electrode as an "intermediate state," whereas at higher voltages, the tunneling particle enters a lower density of states at an energy less than $-\Delta$ for the intermediate state.

Now lower the voltage to $2\Delta/3$. In Fig. 5 the resulting path on the energy diagram is indicated. The particle finally emerges, after three traversals of the barrier via Andreev reflections, into the high density of states at $\Delta$ in the right electrode. This is also a $(T^2)^2$ process. It also occurs at all voltages between $2\Delta/3$ and $2\Delta/2$, but, for these higher voltages, the particle emerges into an energy $E > \Delta$ on the right, hence into a lower density of states. As in the $2\Delta/2$ process, pair currents are generated by the Andreev reflections.

In this way, one concludes that the tunneling conductance should display peaks at $2\Delta/2$ and $2\Delta/3$. The relevant energy diagrams for $2\Delta/5$, $2\Delta/6$, and $2\Delta/7$ are given in Fig. 6. Note that in this $2\Delta/n$ series, when $n$ is even, the peaks are due to entering a high-density-of-states region in the left electrode, while for $n$ odd, the peaks arise from tunneling into the high density of states of the right electrode.

As noted above, the peaks do not appear precisely at these positions, but are shifted relative to the expected positions, the amount of the shift depending upon the value of $n$.

## 7. NUMERICAL RESULTS: ASYMMETRIC JUNCTIONS

For an asymmetric junction there are two variables of interest: $T^2$ and the ratio of gaps. I have scaled all energies relative to the larger of the two gaps, and obtained numerical results in the same approximations as were employed for the symmetric junctions.

Figure 7 shows the dc current versus voltage curves for a junction with $T^2 = 0.42$ and varying values of gap ratio (0.1–0.9). The steplike structures appear to be most pronounced for gap ratios near 0.5. Figure 8 shows the corresponding $dV/dI$ curves. The peaked structures are much more irregular in amplitude and position than are those for a symmetrical junction.

In Fig. 9 the dc current versus voltage curves for a fixed gap ratio of 0.43 (approximately corresponding to the ratio of the energy gap of bulk Sn to that of bulk Pb) are plotted for various values of $T^2$ (from 0.16 to 0.95). Again, as in the symmetric (SIS) case, the sharpness of the step

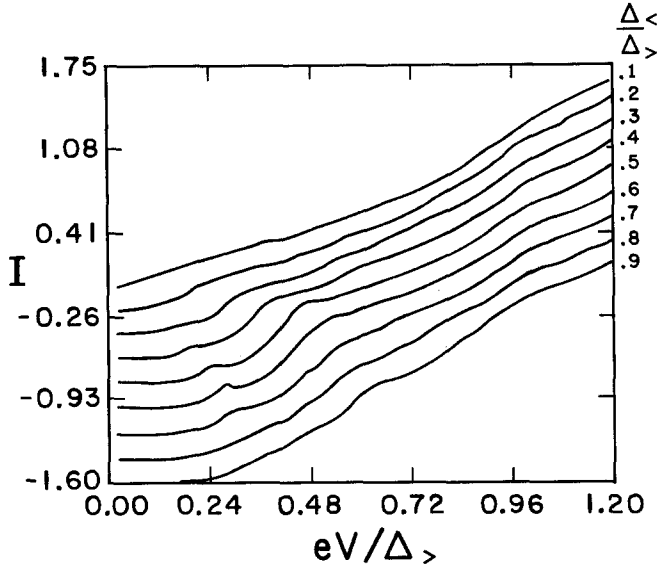


Fig. 7. The dc current versus voltage for gap ratios ranging from 0.1 to 0.9, with $T^2 = 0.42$. Curves are shifted down by 0.2 unit as gap ratio increases.

structure grows as $T^2$ decreases. This can be seen more dramatically in the $dV/dI$ plots, where peaks grow and sharpen as $T^2$ decreases (cf. Fig. 10). The figure for $T^2 = 0.61$ has a striking resemblance to the data of Rowell and Feldman,[14] agreeing in many details with their results.

The KBT analysis can be applied as in the previous section to discover the processes responsible for the structures. However, the asymmetry between the gaps makes the analysis much more tedious. I shall confine my remarks to justifying one prominent qualitative feature.

Consider the behavior of the structure in $dV/dI$ as a function of gap ratio. As can be seen in Fig. 8, there is a qualitative difference between the appearance of the structure for gap ratios greater than 0.5 and ratios less than 0.5. For example, note the great qualitative difference between the structure at a ratio of 0.6 and that at a ratio of 0.4.

To understand this qualitative difference, consider the structure near $\Delta_R - \Delta_L$ (indicated by arrows in Fig. 8), which disappears for gap ratio above 0.5 (in Fig. 8, the arrow in the curve for the gap ratio equal to 0.6 indicates where this structre would be, if it were present). At $\Delta_R - \Delta_L$ one observes that the initial Andreev reflection yields a hole traveling to the left (cf. Fig. 11), which finds accessible states in the left electrode if $\Delta_L < 0.5\Delta_R$. However, if the reverse of this inequality is true, then the initial Andreev

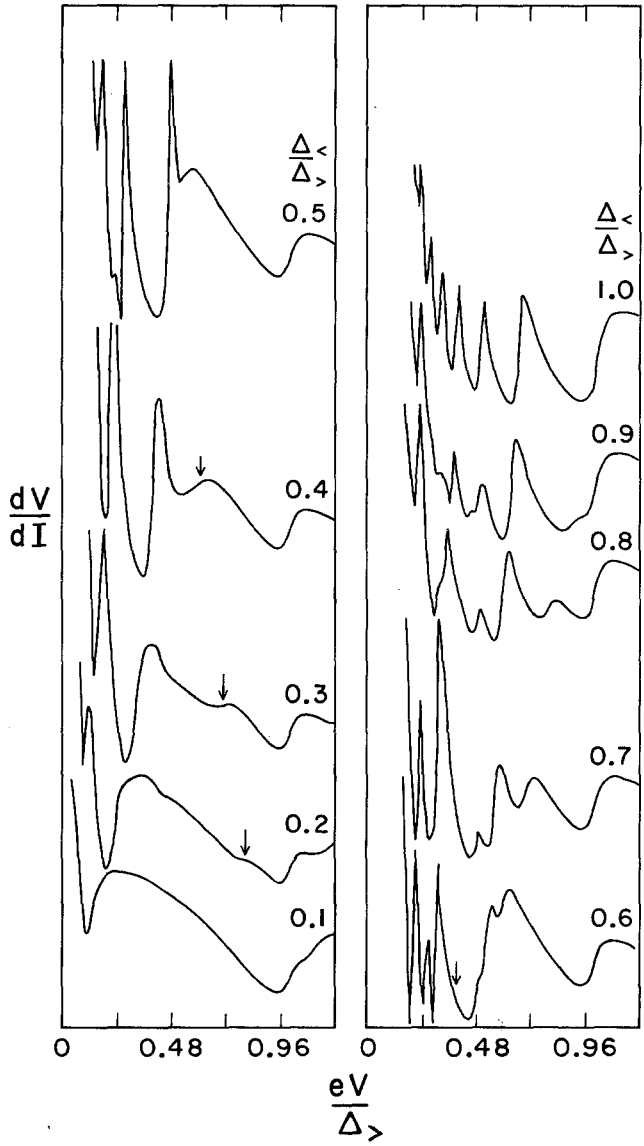


Fig. 8. Dynamical resistance versus voltage for gap ratios from 0.1 to 0.9. Arrows for gap ratios of 0.2, 0.3, and 0.4 indicate structure associated with $\Delta_> - \Delta_<$. Arrow for gap ratio of 0.6 locates position of $\Delta_> - \Delta_<$, where there is evidently no structure. Units along the vertical are arbitrary.

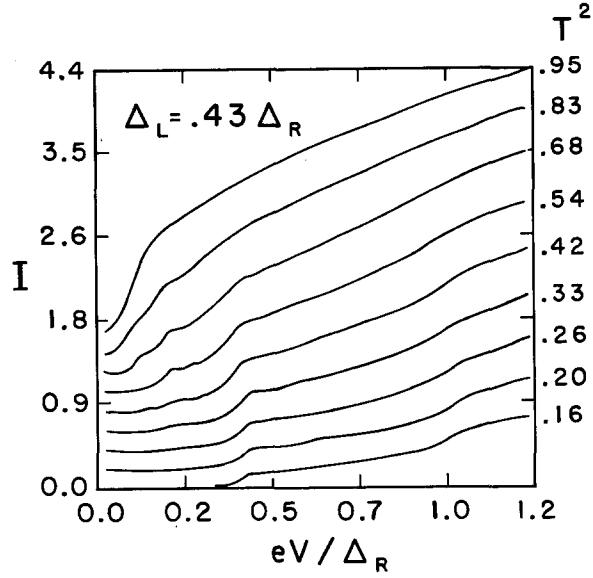


Fig. 9. The dc current versus voltage for gap ratio of 0.43, $T^2$ ranging from 0.16 to 0.95, and successive curves displaced upward by 0.2 along the vertical scale.

reflection yields a particle traveling to the left, and there are no accessible states in the left electrode for this particle, so another Andreev reflection (at least) must occur. More Andreev reflections require more factors of $T^2 < 1$, so the effect of such processes at $\Delta_R - \Delta_L$ is rapidly diminished as $\Delta_L$ increases from $0.5\Delta_R$. Similar arguments apply to the case where $\Delta_R$ is the smaller of the two pair potentials.

The structures appearing in $dV/dI$ and dc current versus voltage curves are all independent of which gap is chosen to be the smaller gap, i.e., the $I$-$V$ characteristics are *symmetrical.*

## 8. AC CURRENT

According to Eq. (37), the ac current is given by

$$\mathrm{Re}\left[\sum_{n\neq 0} J_n(\omega_0)\, e^{in\omega_0 t}\right] \tag{49}$$

The coefficients $J_n$ contain the time-independent portion of the phase $\phi_0$.

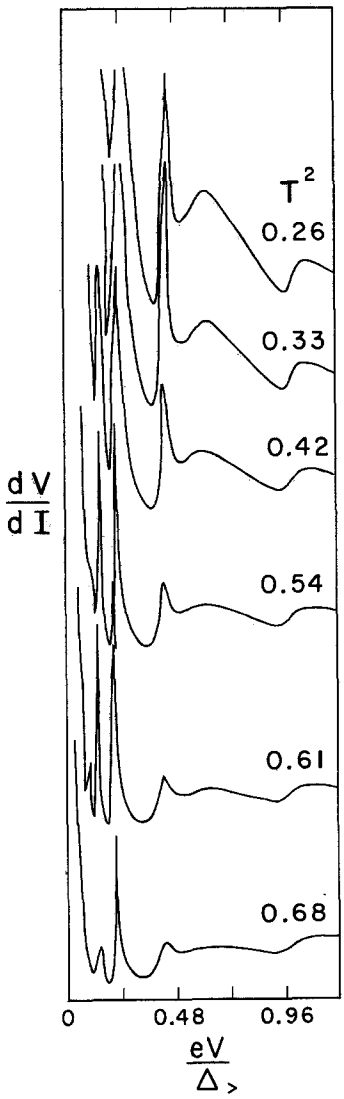


Fig. 10. Dynamical resistance versus voltage for gap ratio of 0.43, $T^2$ from 0.26 to 0.68. Units along the vertical are arbitrary.

Conventionally, for the Josephson effect in ideal junctions, one writes[14]

$$I = I_{qp}(V) + I_{J1}(V)\sin[\phi(t)] + I_{J2}(V)\cos[\phi(t)] \tag{50}$$

where

$$\phi(t) = \phi_0 + \omega_0 t \tag{51}$$

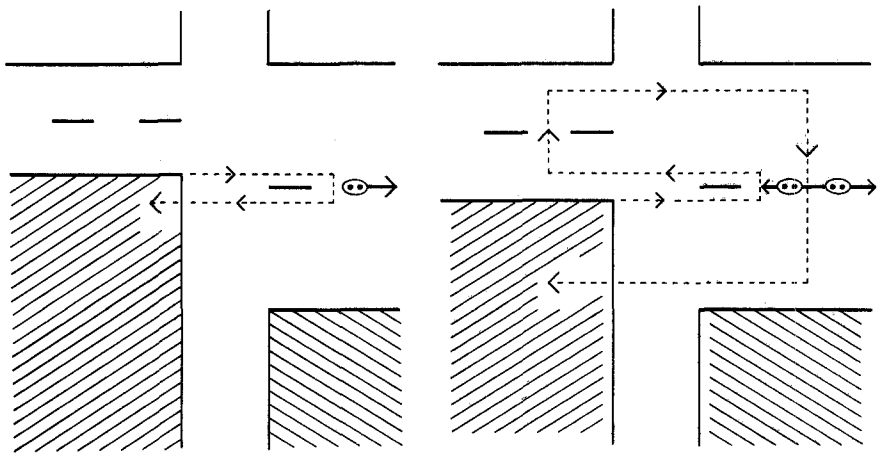

Fig. 11. Semiconductor pictures for (left) $\Delta_L < 0.5\Delta_R$ and (right) $\Delta_L > 0.5\Delta_R$ at $eV = \Delta_R - \Delta_L$, illustrating the qualitative difference between these two cases.

Thus, in order to comply with this convention, I will write Eq. (49) as

$$\begin{aligned}
&\mathrm{Re}\left\{\sum_{n\neq 0}[J_n(\omega_0)\, e^{-in\phi_0}]\, e^{in\phi(t)}\right\} \\
&\quad = \sum_{n>0}\{-\mathrm{Im}(J_n\, e^{-in\phi_0} - J_{-n}\, e^{in\phi_0})\sin[n\phi(t)] \\
&\qquad + \mathrm{Re}(J_n\, e^{-in\phi_0} + J_{-n}\, e^{in\phi_0})\cos[n\phi(t)]\} \\
&\quad = \sum_{n>0}\{I_{J1}(V)_n \sin[n\phi(t)] + I_{J2}(V)_n \cos[n\phi(t)]\} \qquad (52)
\end{aligned}$$

In Figs. 12–15 the amplitudes of the first three of these ac current contributions are plotted versus voltage for $T^2 = 0.13$ (dotted curves), and 0.42 (solid curves), for an SIS junction. For comparison, I have also plotted the results for these quantities in a junction where only the lowest order in $T^2$ need be kept (dashed curves), so that the current takes the form of Eq. (50). It is evident that these ac current versus voltage curves possess structure that is as rich as that of the dc current versus voltage curve. It is remarkable that a *one-parameter* theory ($T^2$) can produce such a variety of structure in the current versus voltage characteristics. The origin of the rich structure in the ac current amplitudes lies in the hopping problem mentioned in Section 5. All of my results flow from the solution to this problem of a particle hopping in a one-dimensional lattice with a site-dependent forward and reverse transfer integral.

The persistence of the second harmonics $I_{J1}(V)_2$ and $I_{J2}(V)_2$ is also remarkable. To my knowledge, these have never been measured by any

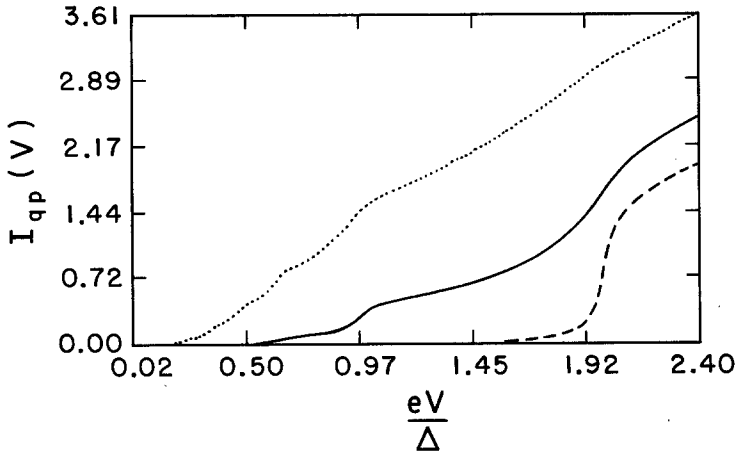


Fig. 12. The dc current $I_{qp}(V)$ versus voltage for a symmetric (SIS) junction with (···) $T^2=0.42$, (—) $T^2=0.13$, and (- -) $T^2$ negligibly small, so that the transfer Hamiltonian result is applicable.

experiment. In junctions with strong subgap structure, these terms must definitely be present. Their observation could provide a useful further test of the present theory.

## 9. DISCUSSION AND CONCLUSIONS

The present theory has, in my opinion, nearly completed the solution to a problem of more than 20 years standing in superconducting tunneling. No previous theory of subgap harmonic structure has achieved the kind of detailed agreement with experiment manifested by this theory. The results of this paper, combined with the physical mechanism of KBT, provide the most complete description yet of superconducting tunnel junctions that exhibit subgap harmonic structure.

In ref. 2 I found that in junctions having one electrode in the normal state the total current could be simply expressed for all voltages as the sum of current due solely to quasiparticles and current due solely to Cooper pairs (supercurrent). There is no such separation in the present case, however. The dc subgap current cannot be written as the sum of currents carried solely by quasiparticles and solely by Cooper pairs. The supercurrent cannot be disentangled from the quasiparticle current because the Andreev reflection processes that allow quasiparticles to carry subgap current through the junction *necessarily* generate or destroy Cooper pairs in the intermediate stages of their Andreev-reflection-assisted tunneling. For this reason, one

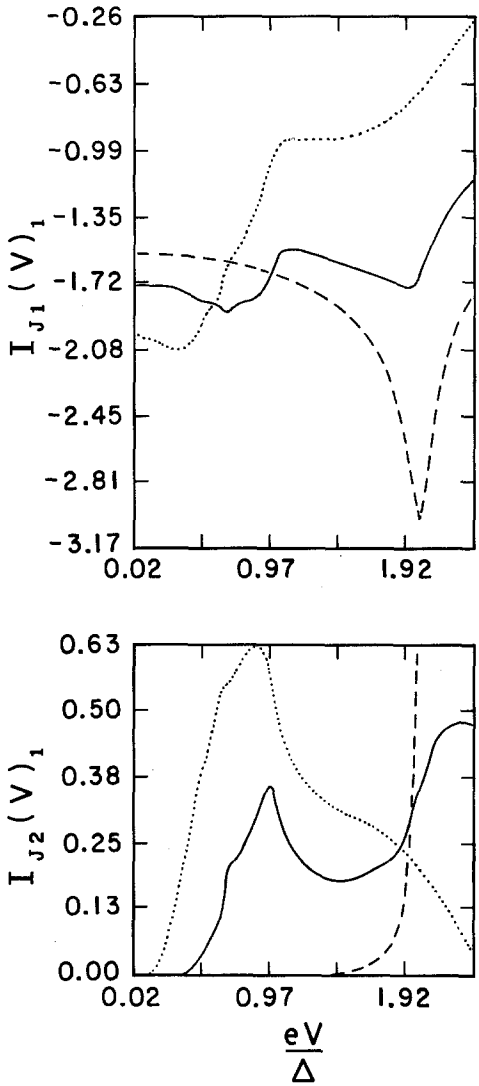


Fig. 13. The ac current amplitudes versus voltage for a current of frequency $\omega_0 = 2eV/\hbar$. The top graph is the amplitude of the sine term (see text), the bottom is that for the cosine term. (- -) The transfer Hamiltonian result; (—) $T^2 = 0.13$; (. . .) for $T^2 = 0.42$.

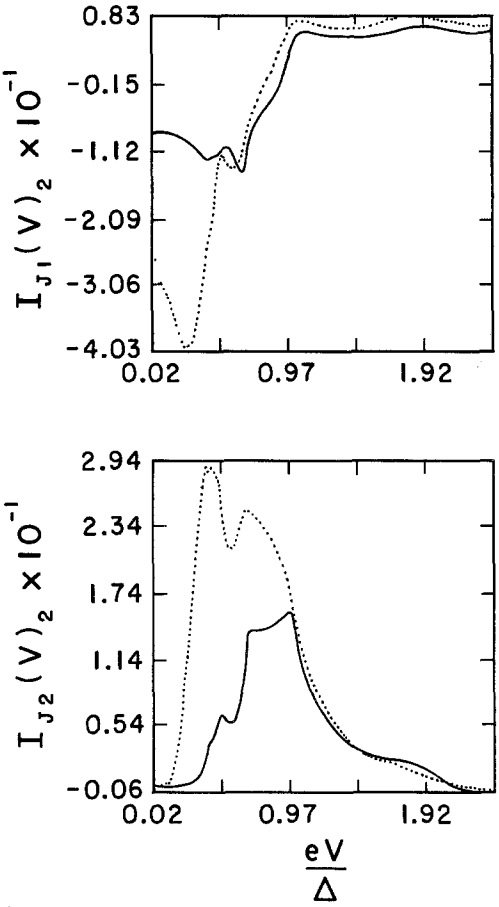


Fig. 14. The ac current amplitudes versus voltage for a current of frequency $2\omega_0$. Top: sine term amplitude; bottom: cosine term amplitude; for (—) $T^2 = 0.13$, (. . .) $T^2 = 0.42$.

cannot extract separate supercurrent and quasiparticle current contributions to the subgap structure.

The parameter $\kappa d_B$, the "barrier thickness parameter," is always less than unity for those junctions that show the clearest subgap structure. Figure 16 shows a graph of barrier height (in meV) versus barrier thickness (in Angstroms) for effective thickness parameters ranging from 0.1 to 1. For barrier heights of the order of an electron volt or more, one can see that *extremely small* values of barrier thickness are implied—in many cases, *unphysically* small values. One can hardly have continuous barrier layers

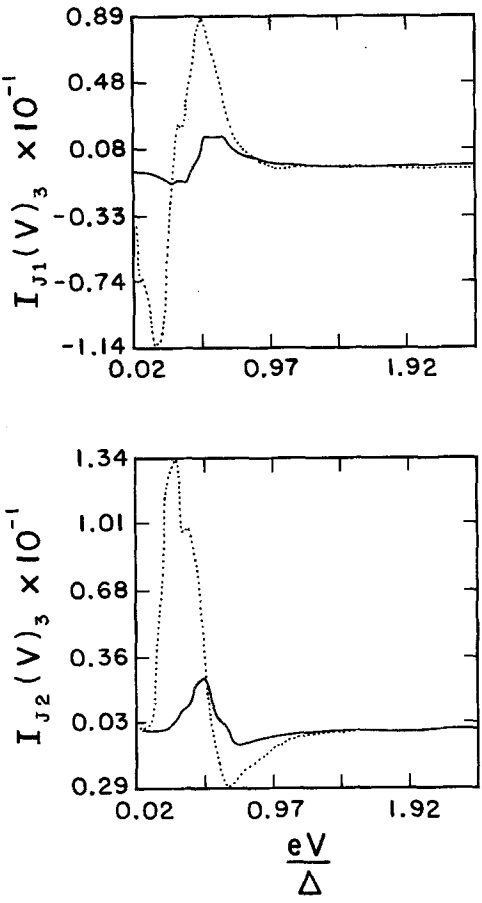


Fig. 15. The ac current amplitudes versus voltage for a current of frequency $3\omega_0$. Top: Sine term amplitude; bottom: cosine term amplitude; for (—) $T^2 = 0.13$, (. . .) $T^2 = 0.42$.

of thickness less than 3 Å or so. It is therefore hard to argue that $\kappa d_B$ be taken literally as determining the thickness and barrier height of a thin insulating layer.

On the other hand, one may regard the barrier transmission process as a generalized scattering process involving two types of scattering: normal scattering, with probability $1 - T^2$, and Andreev scattering. These two types of scattering are accounted for to all orders by the present theory. It is therefore reasonable to suppose that the present results are not specific just to the ideal, continuous, ultrathin-barrier case, but may also apply to

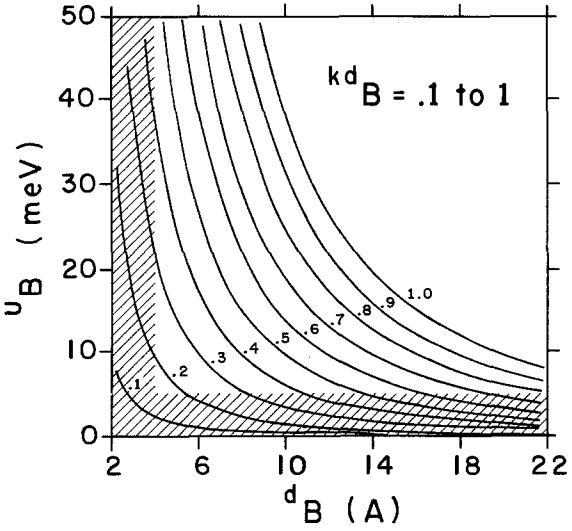


Fig. 16. Barrier height in meV versus barrier thickness in angstroms for various values of $\kappa d_B$. The horizontal shaded region consists of values for which $U_B$ is too small for our approximations to be correct. The vertical shaded region encloses points that correspond to barriers that are too thin to be physically continuous.

"patchy" barriers, as are suspected to be present in many situations. Then $1 - T^2$ would represent the average probability of a single normal scattering in the region of the barrier. Of course, the present theory assumes that the quasiparticle distribution functions in the electrodes are equilibrium functions, but for a patchy barrier, high current densities may be present in the more transparent patches, driving these functions away from their equilibrium values.

I have neglected the effects of capacitance of these junctions, which can lead to voltage fluctuations. Naively, one might suppose that such effects would take the current versus voltage curves presented here and average them over voltage with a Gaussian weighting factor, of width inversely proportional to the capacitance. If this is correct, one would not expect that capacitance plays an important role, except for extremely low-capacitance junctions. The correct inclusion of junction capacitance into the present theory is currently under investigation.

## ACKNOWLEDGMENTS

I thank T. M. Klapwijk for suggesting this calculation, providing encouragement, and making many useful comments on this work, as well

as on that of ref. 2. I also thank W. J. Gallagher, who provided the initial impetus for this work by pointing out its relevance to that of KBT. I am grateful to S. Bermon for further encouragement, and for providing some of his experimental results. I have benefitted greatly from the continuing advice, criticism, and support of W. J. Tomasch, who also provided experimental results for my inspection.

## REFERENCES

1. Gerald B. Arnold, *Phys. Rev. B* **17**, 3576 (1978).
2. Gerald B. Arnold, *J. Low Temp. Phys.* **59**, 143 (1985).
3. T. E. Feuchtwang, *Phys. Rev. B* **10**, 4121 (1974).
4. J. Bardeen, *Phys. Rev. Lett.* **6**, 57 (1961).
5. C. B. Duke, *Tunneling in Solids, Solid State Physics Supplement* (Academic Press, New York, 1969), Vol. 10.
6. B. N. Taylor and E. Burstein, *Phys. Rev. Lett.* **10**, 14 (1963).
7. C. J. Adkins, *Phil. Mag.* **8**, 1051 (1963); *Rev. Mod. Phys.* **36**, 211 (1964).
8. N. R. Werthamer, *Phys. Rev.* **147**, 225 (1966).
9. J. R. Schrieffer and J. W. Wilkins, *Phys. Rev. Lett.* **10**, 17 (1963).
10. T. M. Klapwijk, G. E. Blonder, and M. Tinkham, *Physica B+C* **109 & 110**, 1657 (1982); M. Octavio, M. Tinkham, G. E. Blonder, and T. M. Klapwijk, *Phys. Rev. B* **27**, 6739 (1983).
11. A. F. Andreev, *Sov. Phys. JETP* **19**, 1228 (1964).
12. S. Bermon, private communication.
13. C. Gaffney and W. J. Tomasch, private communication.
14. A. Barone and G. Paterno, *Physics and Applications of the Josephson Effect* (Wiley, New York, 1982).